Quinone Reduction via Secondary B-Branch Electron Transfer in Mutant Bacterial Reaction Centers†

Philip D. Laible,*,‡ Christine Kirmaier,§ Chandani S. M. Udawatte,‡ Samuel J. Hofman,‡ Dewey Holten,§ and Deborah K. Hanson‡

Biosciences Division, Argonne National Laboratory, Argonne, Illinois 60439, and Department of Chemistry, Washington University, St. Louis, Missouri 63130

Received October 7, 2002; Revised Manuscript Received November 25, 2002

ABSTRACT: Symmetry-related branches of electron-transfer cofactors—initiating with a primary electron donor (P) and terminating in quinone acceptors (Q)—are common features of photosynthetic reaction centers (RC). Experimental observations show activity of only one of them—the A branch—in wild-type bacterial RCs. In a mutant RC, we now demonstrate that electron transfer can occur along the entire, normally inactive B-branch pathway to reduce the terminal acceptor Q_B on the time scale of nanoseconds. The transmembrane charge-separated state $P^+Q_B^-$ is created in this manner in a *Rhodobacter capsulatus* RC containing the F(L181)Y-Y(M208)F-L(M212)H-W(M250)V mutations (YFHV). The W(M250)V mutation quantitatively blocks binding of Q_A, thereby eliminating Q_B reduction via the normal A-branch pathway. Full occupancy of the Q_B site by the native UQ_{10} is ensured (without the necessity of reconstitution by exogenous quinone) by purification of RCs with the mild detergent, Deriphat 160-C. The lifetime of $P^+Q_B^-$ in the YFHV mutant RC is >6 s (at pH 8.0, 298 K). This charge-separated state is not formed upon addition of competitive inhibitors of Q_B binding (terbutryn or stigmatellin). Furthermore, this lifetime is much longer than the value of ∼1−1.5 s found when $P^+Q_B^-$ is produced in the wild-type RC by A-side activity alone. Collectively, these results demonstrate that $P^+Q_B^-$ is formed solely by activity of the B-branch carriers in the YFHV RC. In comparison, $P^+Q_B^-$ can form by either the A or B branches in the YFH RC, as indicated by the biexponential lifetimes of ∼1 and ∼6−10 s. These findings suggest that $P^+Q_B^-$ states formed via the two branches are distinct and that $P^+Q_B^-$ formed by the B side does not decay via the normal (indirect) pathway that utilizes the A-side cofactors when present. These differences may report on structural and energetic factors that further distinguish the functional asymmetry of the two cofactor branches.

Dual branches of electron-transfer cofactors are now regarded as common features in reaction centers (RCs)[1], the protein−cofactor complexes that perform the primary reactions in the conversion of photon energy into charge-separated states in photosynthetic organisms. Although controversy exists as to whether one or both of these branches of electron carriers can be active in a particular photosystem, it is clear that only one branch is active in the RCs from purple non-sulfur photosynthetic bacteria. Seventeen years after the solution of the structure of the bacterial RC (*1*), the crystallographic observation of two potential sets of electron transfer cofactors in light of the experimental observations that show activity of only one of them remains an enigma.

In wild-type RCs, the identical sets of cofactors are designated A and B, and only the A branch of cofactors is used for rapid stepwise electron transfer through the protein−cofactor complex to establish a stable charge separation of 30 Å across the lipid bilayer. The cofactors include a specialized dimer of bacteriochlorophyll molecules (P) that serves as the primary electron donor, two monomeric bacteriochlorophyll molecules (B_A and B_B), two bacteriopheophytin molecules (H_A and H_B), two quinone molecules (Q_A and Q_B), and a non-heme iron atom (Figure 1). In the structures of the RCs from *Blastochloris viridis* (*1*) and *Rhodobacter* (*R.*) *sphaeroides* (*2*−*4*), the A and B branches of cofactors are related by an axis of approximate 2-fold symmetry that also extends to the transmembrane helices of the homologous L and M subunits to which the cofactors are bound. In the native photosynthetic membrane, energy transfer from the light-harvesting I complex (LHI) results in formation of P*, the lowest singlet excited state of the dimer. Transfer of an electron to H_A, via B_A, then occurs in ∼3 ps. The $P^+H_A^-$ state decays in ∼200 ps by forward transfer of an electron to form $P^+Q_A^-$ (*5*), followed by formation of $P^+Q_B^-$ in 1−200 μs (*6*−*8*). Following two successive turnovers of Q_A, Q_B becomes doubly reduced and acquires two protons that are transported from the cytoplasm

† Supported by the United States Department of Energy, Office of Biological and Environmental Research, under Contract W-31-109-ENG-38 (P.D.L., C.S.M.U., S.J.H., and D.K.H.). C.K. and D.H. were supported by Grant MCB0077187 from the National Science Foundation.

* Author to whom correspondence should be addressed. E-mail: laible@anl.gov.

‡ Argonne National Laboratory.

§ Washington University.

[1] Abbreviations: P, bacteriochlorophyll dimer; B_A and B_B, monomeric bacteriochlorophylls; H_A and H_B, bacteriopheophytins; *β*, bacteriochlorophyll incorporated for bacteriopheophytin at the H_A site; Q_A and Q_B, primary and secondary quinone acceptors; fs, femtosecond; ps, picosecond; ns, nanosecond; μs, microsecond; ms, millisecond; s, second; RC, reaction center; Q, quinone; UQ, ubiquinone; MK, menaquinone.

10.1021/bi026959b CCC: $25.00
Published on Web 01/22/2003

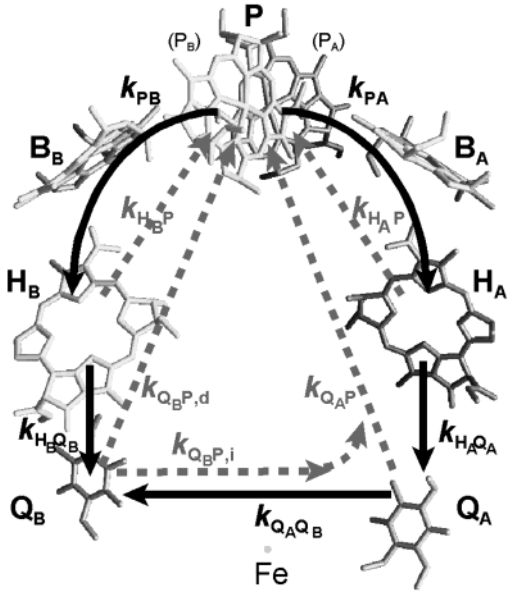

FIGURE 1: Pathways within the bacterial photosynthetic reaction center for forward electron transfer (solid) and charge recombination (dashed). Cofactors are labeled as described in the text and are displayed as found in the 2.7 Å X-ray structure of the *R. sphaeroides* reaction center (*4*). The forward rate of electron transfer from Q_A to Q_B represents that for transfer of the first electron [normally depicted as $k_{Q_AQ_B}$ (*1*)]. This study does not involve transfer of the second electron to Q_B [$k_{Q_AQ_B}$ (*2*)].

through the protein matrix to the buried Q_B site. Q_BH_2 diffuses from the RC and is replaced by oxidized UQ_{10} from the intermembrane pool. The rates at which the charge-separated states $P^+Q_A^-$ and $P^+Q_B^-$ recombine (k_{Q_AP} and $k_{Q_BP,i}$, respectively) differ by at least 1 order of magnitude in wild-type RCs. The $P^+Q_B^-$ state decays by charge recombination in ~1−1.5 s, depending upon pH, whereas the lifetime of the $P^+Q_A^-$ state is ~100 ms when forward electron transfer to Q_B is blocked (as reviewed in refs *9* and *10*).

No photobleaching of spectral features assigned to B_B or H_B is observed in wild-type RCs indicating that these cofactors are not active as electron carriers (for reviews see refs *11* and *12*). It is not known whether the B-side cofactors are vestigial, whether they play an important role in maintaining the overall RC architecture, or whether the differentiation of the two pathways was selected during evolution of the photosynthetic apparatus. Likewise, the factors that lead to the observed unidirectional electron flow are only beginning to be understood. Asymmetries in the protein are thought to give rise to both differences in free energies of the charge-separated states and in the electronic couplings between the cofactors on the active and inactive branches. The extent to which electronic factors complement demonstrated effects of energetics in governing directionality is one focus of work in the field (*12*−*27*).

The cofactors of the B branch can be coaxed into participating in light-induced electron-transfer reactions by using photochemical trapping conditions (*14*), high photon energies or fluxes (*28*, *29*), or site-specific mutagenesis (*18*, *24*, *26*, *30*−*35*). Substantial B-branch primary electron transfer has now been conclusively demonstrated in RCs of *R. capsulatus* and *R. sphaeroides* where protein engineering has been used to manipulate the relative energy levels of A- and B-side cofactors (*18*, *24*, *26*, *30*, *31*, *34*). In general, the amount of B-side electron transfer is smaller in RCs of *R. sphaeroides* when compared to RCs of *R. capsulatus* harboring the equivalent mutations (*33*).

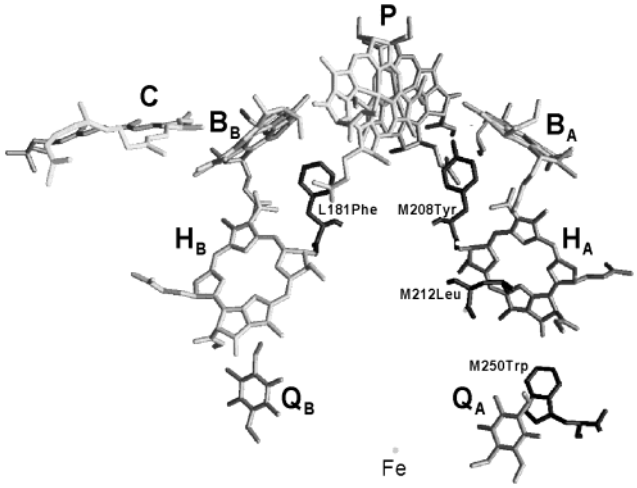

FIGURE 2: Structural positions of the substituted amino acids in engineered reaction centers of this study, in relation to the A-branch and B-branch cofactors (*4*).

Recently, the primary charge separation processes in *R. capsulatus* RCs bearing the F(L181)Y-Y(M208)F-L(M212)H mutations (YFH) were reported (*26*). The L181Phe-M208Tyr pair of symmetry-related residues represents a conserved asymmetry that contributes to the differentiation of the inactive and active branches of cofactors, respectively (Figure 2; refs *16*, *19*, *20*, and *36*−*49*). Reversal of the asymmetry produces an RC in which the Y(M208)F substitution is thought to raise the free energy of $P^+B_A^-$ (placing it very close to or slightly above P*; Figure 3) such that electron transfer along the A branch of cofactors is less favorable. Similarly, the F(L181)Y substitution is suggested to lower the free energy of $P^+B_B^-$, thus promoting electron transfer via the B branch of cofactors. The L(M212)H mutation provides a Mg ligand near the binding site of H_A (Figure 2), resulting in the incorporation of a bacteriochlorophyll molecule (designated β). This substitution slows electron transfer to the A branch and opens a convenient spectral window in the 500−580 nm region for monitoring electron transfer to the B-branch cofactor H_B. The combination of mutations in the YFH RC causes branching of photochemistry from P* to yield approximately 30% electron transfer to H_B.

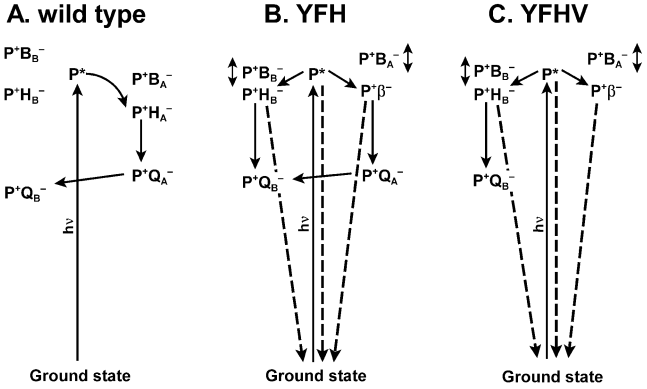

FIGURE 3: Schematic diagrams showing relative energy levels of charge-separated states and pathways for charge separation and competing reactions that lead to long-lived P^+Q^- signals in wild-type and mutant RCs of this study. The double-headed arrows on some states reflect uncertainty as to whether these states are slightly above or slightly below P*.

Table 1: Plasmids and Strains Used in This Study

plasmid or strain	description	source
	Plasmids	
pUHTMluBgl	broad-host-range plasmid carrying wild-type *puf* operon; L and M genes marked with silent *Mlu*I and *Bgl*II sites, respectively; pU2922 derivative (*54*); $Ap^RKm^RTc^R$	this study
pUHTYFH	F(L181)Y-Y(M208)F-L(M212)H mutations; pUHTMluBgl derivative; $Ap^RKm^RTc^R$	this study
pUHTYFHV	F(L181)Y-Y(M208)F-L(M212)H-W(M250)V mutations; pUHTMluBgl derivative; $Ap^RKm^RTc^R$	this study
pUHTFHV	Y(M208)F-L(M212)H-W(M250)V mutations; pUHTMluBgl derivative; $Ap^RKm^RTc^R$	this study
pUHTMluBgl:α^-	pUHTMluBgl derivative carrying $His^{32} \rightarrow$ Arg mutation that prevents assembly of LHI complex (*55*); wild-type RC genes; $Ap^RKm^RTc^R$	this study
pUHTYFH:α^-	F(L181)Y-Y(M208)F-L(M212)H mutations; pUHTMluBgl:α^- derivative; $Ap^RKm^RTc^R$	this study
pUHTYFHV:α^-	F(L181)Y-Y(M208)F-L(M212)H-W(M250)V mutations; pUHTMluBgl:α^- derivative; $Ap^RKm^RTc^R$	this study
pUHTFHV:α^-	Y(M208)F-L(M212)H-W(M250)V mutations; pUHTMluBgl:α^- derivative;$Ap^RKm^RTc^R$	this study
	Strains	
E. coli		
S17-1	*recA pro hsdR* RP4-2-Tc::Mu-Km::Tn7	ref *56*
R. capsulatus		
U43	*puc puf*:: $\Omega St^R/Sp^R$; recipient for above broad-host-range expression plasmids	ref *57*

Earlier experiments that have probed for evidence of electron transfer from H_B^- to Q_B utilized RCs in which the initial yield of $P^+H_B^-$ formation was at most one-half of the 30% obtained in the YFH RC (*30*, *35*). These experiments were also complicated by the fact that Q_B is loosely bound, and historical LDAO-based purification protocols yielded samples in which most of the RCs had unoccupied Q_B binding pockets (*50*, *51*). Thus, excess ubiquinone was added to reconstitute the Q_B site. However, reconstitution methods often fail to do so quantitatively and reproducibly, particularly (in our experience) at the high RC concentrations needed to carry out ultrafast transient absorption measurements in parallel with the slower kinetic studies to uniformly probe the formation and decay of $P^+Q_B^-$. Furthermore, kinetic studies have indicated that structural changes in the Q_B binding domain occur upon its reconstitution with exogenous quinone (*7*). Experiments to monitor secondary electron transfer via A-side cofactors do not suffer from similar challenges because Q_A is bound more tightly and is quantitatively retained during purification of RCs having a native Q_A binding pocket (*52*, *53*).

We have combined some of the RC properties that are necessary to allow unambiguous demonstration of secondary B-side electron transfer leading to Q_B reduction in designing the YFHV mutant RC reported here. The population of $P^+Q_B^-$ that forms in the YFH RC would be expected to be a mixture of that formed solely from B-side cofactors and that formed from A-branch electron-transfer involving $P^+Q_A^-$ as its precursor, if indeed both secondary electron transfer pathways are active. By incorporating the W(M250)V mutation that quantitatively blocks binding of Q_A, we eliminated the formation of $P^+Q_B^-$ via the normal A-branch pathway. To achieve full occupancy of the Q_B site by the native UQ_{10} and avoid the necessity of its reconstitution by exogenous quinone, RCs were purified with a new protocol that employed a mild detergent, Deriphat 160-C. We present results that demonstrate conclusively that the B-branch pathway operates in this sample to reduce the terminal electron acceptor Q_B on the time scale of nanoseconds. The lifetime of the resulting $P^+Q_B^-$ charge-separated state is >6 s (at pH 8.0, 298 K). This long-lived signal is lost with the addition of competitive inhibitors of Q_B binding (such as terbutryn or stigmatellin) that block formation of $P^+Q_B^-$. The properties of this $P^+Q_B^-$ state, formed solely by activity of the B-branch carriers, are compared to the properties of $P^+Q_A^-$ and to those of $P^+Q_B^-$ formed by the normal activity of the A-branch cofactors in the native or less extensively modified RCs. These results demonstrate unequivocally that the B-side electron-transfer pathway is capable of creating a productive, long-lived charge separation that spans the membrane.

EXPERIMENTAL PROCEDURES

Mutant Construction. Plasmids and strains used in this study are listed in Table 1. The code used to identify the mutant residues in the RCs is as follows: Y = F(L181)Y; F = Y(M208)F; H = L(M212)H; and V = W(M250)V. Construction of the F(L181)Y-Y(M208)F-L(M212)H triple mutant—YFH—was described previously (*26*). The W(M250)V mutation was introduced via site-specific mutagenesis (Chameleon kit, Stratagene) of a wild-type M gene subcloned into pBS^- (Stratagene). Correct candidates were identified by loss of a *Hae*II site at M250, and the mutation was further confirmed by dideoxy sequencing according to instructions from a kit (Sequenase 2.0, United States Biochemical). The mutation encoding the Val at M250 was linked with the other two changes in the FH-mutant M gene by replacement of a wild-type *Bst*EII−*Bam*HI fragment with the equivalent fragment from the W(M250)V mutant plasmid, screening again for the loss of the *Hae*II site at M250. To generate the YFHV mutant RC of *R. capsulatus*, this mutant M gene was coupled to the L gene carrying the F(L181)Y mutation.

Mutant L and M genes were returned to the *puf* operon in derivatives of broad-host-range plasmid pU2924 (*54*) for expression in *R. capsulatus*. These derivatives, designated pUHTMluBgl or pUHTMluBgl:α^-, contained a sequence encoding a C-terminal hepta-histidine tag that had been added to the gene for the M subunit (P. D. Laible and D. K. Hanson, unpublished experiments). Plasmid pUHTMluBgl:α^- carried a mutation in the *puf*A gene ($His^{32} \rightarrow$ Arg; ref *55*) that prevented formation of the LHI complex. In addition, the L and M genes in these two plasmids were marked with silent, unique restriction site tags (*Mlu*I at codons L144-L145, *Bgl*II site at codons M86-M87) facilitating shuttling of the mutant genes into these plasmids. Mutant L genes were subcloned into these plasmids as *Hin*dIII−*Kpn*I fragments, and mutant M genes were introduced as *Kpn*I−*Bam*HI fragments. The swaps were confirmed by loss of the *Mlu*I and/or *Bgl*II restriction sites.

Broad-host-range plasmids carrying mutant RC genes were transferred from *E. coli* donor strain S17-1 (*56*) to *R. cap*

sulatus deletion strain U43 (LHI$^-$LHII$^-$RC$^-$; ref *57*) by conjugation, and transconjugants were selected on RCV medium (*58*) containing kanamycin (30 μg/mL). Strains were routinely propagated on ^{Super}RCVPY medium (*33*) under chemoheterotrophic conditions in the dark (34 °C), in the absence of selection for RC function.

Purification of Reaction Centers. RCs were purified typically from 2 L cultures of *R. capsulatus* strains. Cells were harvested, then washed and resuspended in a minimal volume of buffer 1 (10 mM Tris, pH 8.0, 100 mM NaCl). The cell suspension was sonicated in the presence of DNase and lysed by passage through a French press. Following low speed centrifugation (25 000*g*, 10 min) to remove cell debris, the lysate was treated in the following manners, depending on the detergent used for extraction:

(A) Deriphat 160-C. Lysates of cells lacking the LHI complex (expressed from derivatives of pUHTMHBgl:α^-) were diluted in buffer 1 to an $A_{800} = 1$. A 30% solution of Deriphat 160-C was added dropwise with stirring to a final concentration of 1%. [Deriphat 160-C (30% solution) and Deriphat 160 (solid) were generous gifts of Cognis Corporation, Hoboken, NJ]. The solution was stirred at room temperature for 1 h, and remaining membrane fragments were removed by ultracentrifugation (240 000*g*, 1.5 h). The membrane extract was bound in batch mode by incubation with Ni−NTA agarose resin (Superflow, Qiagen, Inc.; Valencia, CA) that had been equilibrated with buffer 2D (10 mM Tris, pH 8.0, 0.1% Deriphat 160-C, 50 mM NaCl). Ten mL of resin was used per liter of cell culture, and the suspension was incubated on an inverter for 1 h at 4 °C. The membrane−resin solution was then transferred to a column, and the bed was washed with buffer 2D until the A_{280} of the eluate dropped below 0.1. His-tagged RCs were eluted from the column with buffer 3D (10 mM Tris, pH 8.0, 0.1% Deriphat 160-C, 100 mM NaCl, 100 mM imidazole). Pure RCs were washed with buffer 4D (10 mM Tris, pH 8.0, 0.1% Deriphat 160-C, 100 mM NaCl) using a spin concentrator (Ultrafree Biomax; Millipore; Bedford, MA) with a 50 kDa cutoff filter in a centrifuge operating at 2000*g* to dilute serially the imidazole from the samples and concentrate them for transient absorption spectroscopy.

(B) LDAO. Lysates of cells containing both LHI and RC complexes (expressed from derivatives of pUHTMHBgl) were diluted in buffer 1 to an $A_{875} = 10$ and warmed to 30 °C. Imidazole was added (5−10 mM), and LDAO (30% solution, Fluka) was introduced dropwise, with stirring, to a final concentration of 1%. The solution was incubated at 30 °C with agitation for 10−15 min, and remaining membrane fragments were removed by ultracentrifugation (240 000*g*, 1.5 h). The membrane extract was bound in batch mode by incubation with Ni−NTA agarose resin that had been equilibrated with buffer 2L (10 mM Tris, pH 7.8, 0.05% LDAO). Four mL of resin was used per liter of cell culture, and the suspension was incubated on an inverter for a minimum of 30 min at 4 °C. The membrane−resin solution was then transferred to a column, and the bed was washed with buffer 2L until the A_{280} of the eluate dropped below 0.1. His-tagged RCs were eluted from the column with buffer 3L (10 mM Tris, pH 7.8, 0.05% LDAO, 40 mM imidazole). Pure RCs were washed with buffer 2L and concentrated as described above.

Quinone Reconstitution. Concentrated stock solutions of UQ_6 were prepared in 10 mM potassium phosphate buffer (pH 8.0) containing 0.8% Triton X-100, and full occupancy of the Q_B site was obtained by the addition of 30 equiv of quinone. Terbutryn stock solutions were prepared in 10 mM potassium phosphate buffer (pH 8.0) containing 0.5% Triton X-100, and the number of equivalents needed for >95% inhibition of Q_B binding was titrated (vide infra). Optimal incorporation occurred in RC samples containing 100 mM NaCl and required heating of the concentrated stock of quinone or inhibitor to ∼50 °C in a water bath or microwave prior to its addition to the RC sample. After thorough mixing, the sample was incubated at 28 °C for 20 min to promote full incorporation. The final concentration of Triton X-100 was kept below 0.05% to reduce the risk of denaturing RCs or partitioning of the quinone (or inhibitor) into detergent micelles instead of protein.

μs → s Spectroscopy. The lifetimes of long-lived charge-separated states were determined on a laboratory-designed single-beam spectrophotometer. All measurements were made at 298 K. The 860 (±5) nm measuring beam was supplied by a 100 W quartz-halogen lamp passing through a monochromator. The intensity was reduced with a series of neutral density filters to minimize actinic effects while preserving acceptable signal-to-noise levels (S/N; vide infra). Rates of $P^+Q^- \rightarrow PQ$ charge recombination were measured by recording, on a digitizing oscilloscope (TDS 3012B, Tektronics), the intensity of the bleach of the ground-state band of P at 865 nm as a function of time following excitation with a 7-ns 532-nm 90-mJ pulse from a Q-switched frequency-doubled Nd:YAG laser (DCR-3, Spectra-Physics). Samples (typical volume of 200 μL) were placed in a cuvette with a path length of 2 mm placed at 45° relative to the excitation and probe pulses. Excitation of the sample was controlled by manually triggering the laser Q-switch. The repetition rate of data acquisition was varied depending on the transient lifetimes of the P^+Q^- states; it never exceeded one per minute and was often less than one per five minutes. To allow complete recovery of the ground state, a shutter in the measuring light path blocked the beam and its actinic effects in the time between data acquisitions. Data are reported for concentrated (∼20 μM) RC samples matching the conditions that are typically used for ultrafast experiments, laying groundwork for such experiments that we will report elsewhere (*59*). However, several measurements were made with more dilute RCs (1−3 μM RCs, the typical concentration found in the literature for studies of the P^+Q^- states), with similar results. Three types of samples were routinely examined: (1) Deriphat-purified RCs taken directly from column chromatography, (2) LDAO-purified RCs with added quinone (30−40 UQ_6 equiv, sufficient to reconstitute the Q_B binding pocket), and (3) both types of RCs with added inhibitor. For quantitative inhibition, terbutryn or stigmatellin (500 μM; 25 equiv) were added for determination of the $P^+Q_A^-$ lifetime in the absence of forward electron transfer to Q_B.

Considerable effort was spent on the design/modification of the ultraslow apparatus for these experiments with concentrated RC samples. The S/N ratio of long-lived P^+Q^- kinetics was maximized while minimizing the detrimental actinic effects of the measuring light during the long time of data acquisition (in some cases up to 2 min). For wild-

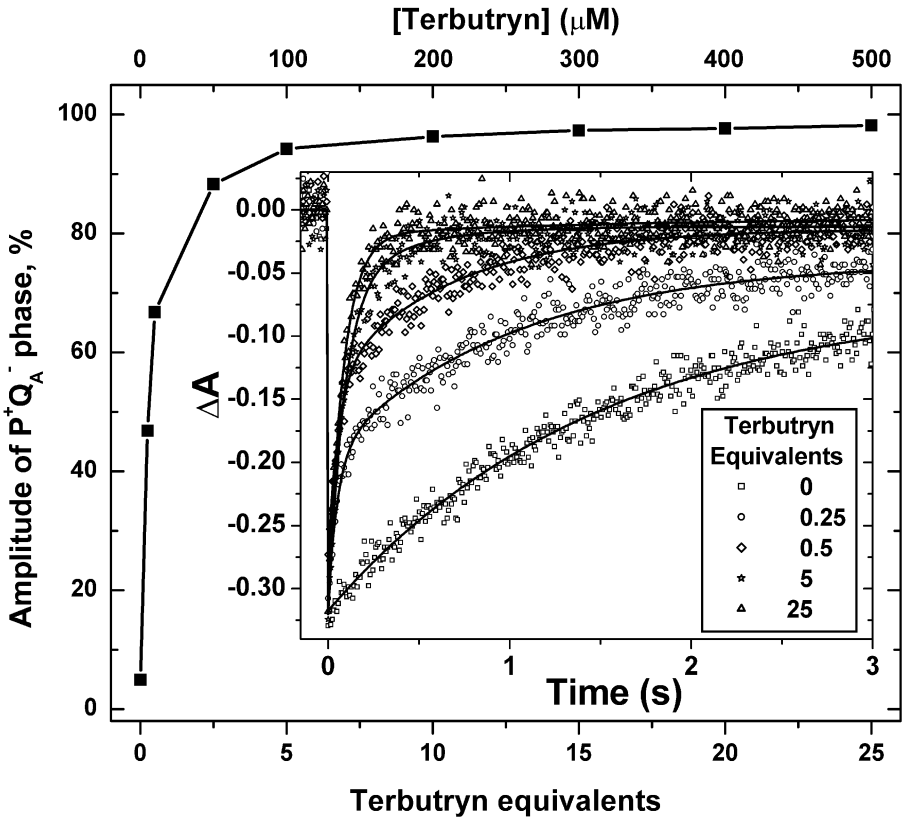

FIGURE 4: Effect of terbutryn—a competitive inhibitor of Q_B binding—on the relative amount of the fast phase of charge recombination of P^+Q^- states in wild-type RCs. In subsequent experiments, 25 equiv of terbutryn were used to prevent formation of $P^+Q_B^-$. The reduction in the amplitude of an actinic effect of the measuring light can be observed in samples containing increasing amounts of terbutryn (inset).

Table 2: Lifetimes and Yields of P^+Q^- States in Various Mutant RC Purified Using the Detergent Deriphat 160-C (Unless Otherwise Noted)

	Recombination[a]		yield[b] of $P^+Q_B^-$	yield[c] of actinic
strain name	$P^+Q_A^-$ (ms)	$P^+Q_B^-$ (s)	(%; 298 K)	signal (%)
WT (LDAO)	90	1.3	~80	12
WT	90	1.5	100	13
YFH	80	0.8 (60%) 6.1 (40%)	79	6
YFHV	not obs	>10	32	3

[a] Not obs = no signals seen for this reaction. [b] ±3% error, not including recycling phenomenon discussed in the text. [c] Amplitude of the constant extracted from the nonlinear analysis of the ultraslow kinetic data (expressed as percentage of the full bleach of the wild type) from LDAO-purified RCs in the presence of quinone or Deriphat-purified RCs following affinity chromatography. Actinic signals were absent in inhibited RCs.

type RCs with fully occupied Q_B sites, the measuring beam could only be attenuated to levels where signals at >10 s following excitation were ≤14% of pre-trigger levels while preserving S/N at acceptable levels (Table 2).

While performing terbutryn titration experiments, it became obvious that the observed actinic effects scaled with the activity of the RCs in forming P^+Q^- states; effects were especially prevalent in wild-type RCs. As inhibitor concentration increased, the actinic-induced bleach, at long times, was dramatically reduced (Figure 4, inset). With sufficient terbutryn, the actinic effects were quantitatively eliminated—suggesting that the $P^+Q_B^-$ state was the prime contributor to the residual signal and that the $P^+Q_A^-$ state of significantly shorter lifetime was less of a problem. The actinic effect also could be reduced by mutation (e.g., W(M250)V; Table 2).

In our analysis of the data, we chose not to correct for the actinic effects that we observed (Table 2) because the actinic signal was impossible to predict, and was not reproducible in control experiments less the pump pulse and linear approximation corrections resulted in nonexponential kinetic profiles. Therefore, we fitted the uncorrected, long-lived P^+Q^- signals. We estimate that the error in the lifetimes is no more than 15%; this error has no impact on the interpretations given below. Where applicable, we report the amplitude of the long-lived actinic signal for every measurement that was carried out in the absence of inhibitor. The initial P^+Q^- signal amplitudes that we observed in this experimental configuration are not significantly perturbed by the actinic effect since the measuring beam had little time to elicit its influence promptly after the shutter in the probe beam was opened—especially as signal amplitudes were always extracted from initial data recorded on a 40 ms/div time base.

The calculated ΔA was fitted to a single- or double-exponential function plus a constant using the nonlinear curve fitting routines built into the software package Origin (Microcal Software, Inc.). In most cases, kinetic traces were fitted individually, but lifetimes of states reported include averages over measuring replications and data acquisition at different time bases of the digitizing oscilloscope.

RESULTS AND DISCUSSION

Mutant Design. The residues that were substituted and their structural positions relative to the cofactors (*4*) are shown

in Figure 2. Our goal was to construct a mutant RC in which B-branch electron-transfer yielding $P^+Q_B^-$ could be observed unambiguously. Therefore, we needed to combine mutations that were known to (a) enable activity of B-branch cofactors, (b) clear the Q_x region of the spectrum such that charge-separated states involving B-branch cofactors could be readily observed and assigned, and (c) quantitatively disable formation of $P^+Q_B^-$ via A-branch electron transfer.

The substitutions in the YFH mutant RC accomplish all but the third goal (c). While the F(L181)Y-Y(M208)F-L(M212)H mutations cause a significant decrease in the yield of $P^+Q_A^-$ in this RC (*26*), 100% of that state can be converted to $P^+Q_B^-$ by subsequent forward electron transfer. To eliminate formation of $P^+Q_B^-$ via A-branch cofactors, we targeted residue M250Trp (M252 in *R. sphaeroides*) for mutagenic replacement. This residue is in van der Waals contact with H_A and Q_A and has been suggested to function as a conduit for electron transfer between these two cofactors (*60*). Its mutation to Val has been shown to result in quantitative loss of Q_A from RCs of *R. capsulatus* (*61*) and *R. sphaeroides* (*62*, *63*). Previous studies suggested that no significant structural change occurred with a variety of substitutions at this site since all of the mutant RCs were capable of performing light-induced charge separation if enough quinone was added (*64*). Binding of Q_A was reduced most substantially by mutation of Trp to Glu, Val, and Arg; it was shown that the K_D for MK_0 in the valine mutant RC rose from the wild-type value of <1 to 240 μM (*64*).

LDAO is widely used for the purification of RCs; however, we investigated several milder detergents—including Deriphat 160-C—after finding that LDAO was often too harsh for the purification of some RCs that carry multiple engineered mutations. During a 1-h incubation at room temperature, a 1% solution of Deriphat 160-C is so mild that it is incapable of dissociating the LHI complex from the RC in membranes that carry both complexes. The same conditions, however, could be used successfully for extraction and purification of RCs from membranes of strains that were devoid of light-harvesting complexes. Therefore, the wild-type and mutant RCs of this study that were Deriphat-purified were expressed from genes that were subcloned into a *puf* operon carrying a mutation in the *puf*A gene ($His^{32} \rightarrow Arg$; ref *55*) that prevents assembly of the LHI complex (Table 1).

Ground-State Absorption Spectra. Absorption spectra recorded at room temperature are shown in Figure 5 for the RCs used in this study. The use of 1% LDAO for the extraction of RCs from the intracytoplasmic membrane causes a shift in the lowest energy band of P from its native position at 870 to 850 nm. It was shown previously that the spectral shift in the position of the P band is due to changes in the electronic structure of the dimer that are presumably caused when native charged phosholipids of the cell membrane that interact with P are replaced by detergent molecules (*51*). The difference in the electronic structure of P is reflected in ENDOR spectra that show an increase in the asymmetry of the spin distribution over the two bacteriochlorophyll molecules (P_A and P_B, Figure 1) of the dimer (*65*, *66*). Use of the milder detergent Deriphat 160-C for solubilization of membranes yielded wild-type and mutant RCs in which the P band remained at the native 870 nm position.

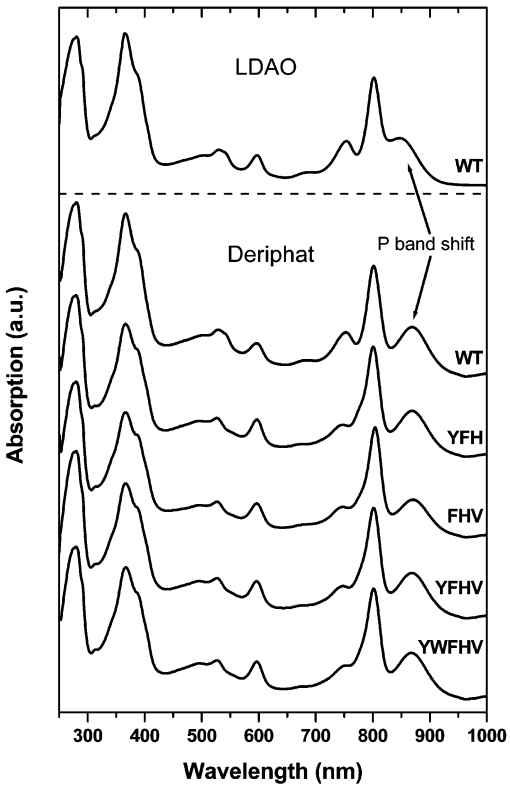

FIGURE 5: Spectra of purified mutant reaction centers, normalized at either 850 (LDAO) or 870 nm (Deriphat), and displaced for comparison. Note the relative positions of the lowest energy band of P [~850 nm in LDAO-purified RCs; ~870 nm in Deriphat-purified RCs (arrows)] and the differences in spectral features at 780, 760, 590, and 545 nm that are associated with the β phenotype (see text).

The β phenotype is clearly exhibited in all strains containing the M212Leu → His substitution (YFH, FHV, and YFHV) and is characterized by a higher A_{800}/A_{870} ratio than in the wild type, an asymmetric monomeric bacteriochlorophyll band at ~800 nm because of the presence of the absorption band of β at ~780 nm, loss of the Q_x absorption band of H_A at 545 nm, and an increase in absorption in the Q_x region of β (~590 nm). The F(L181)Y and Y(M208)F mutations have minimal effects on the ground-state spectra (*47*), and no effects of the W(M250)V mutation are visible.

Deriphat-Purified RCs Quantitatively Retain Q_B. Because of the differences between the expected rates for $P^+Q_A^-$ and $P^+Q_B^-$ recombination (reviewed in refs *9* and *10*), we chose to characterize P^+Q^- recombination kinetics as a probe for formation of $P^+Q_B^-$ via B-side electron transfer in our series of mutant RCs. It has long been known that the Q_B site is unoccupied in the majority of RCs present in a sample purified with a relatively high concentration (1%) of LDAO (*50*, *51*). The transient kinetics shown in the inset of Figure 6 (solid symbols, wild-type RCs) reflect a mixture of long-lived and short-lived P^+Q^- states that is characteristic of such a sample. The data were best fitted with two exponentials. The majority of the signal disappears with a lifetime of ~100 ms, and thus is consistent with recombination of the short-lived $P^+Q_A^-$ state. The remaining 30% of the charge recombination occurs with a time constant of ~1.5 s, and this process is assigned to recombination of the relatively long-lived $P^+Q_B^-$ state (in the fraction of RCs containing Q_B). Reconstitution of the Q_B site with UQ_6 changes the

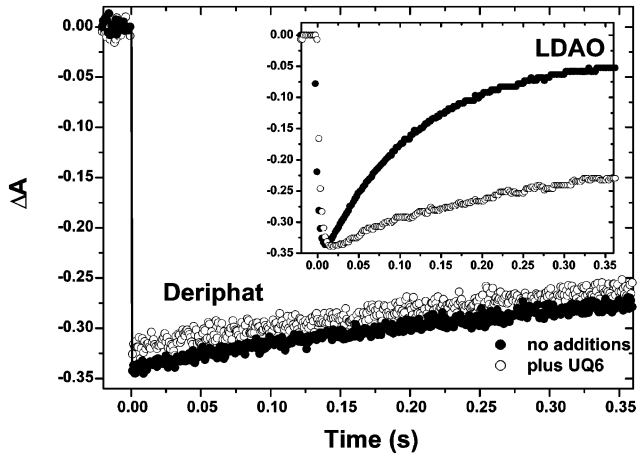

FIGURE 6: Effect of quinone (UQ_6) addition on the amplitudes and lifetimes of P^+Q^- states in the wild-type *R. capsulatus* RC isolated using either Deriphat 160-C (main panel) or LDAO (inset). The concentration of RCs was ~20 μM.

kinetics such that >80% of the signal decays with the longer time constant of ~1.5 s that is characteristic of $P^+Q_B^-$ charge recombination.

In contrast, a single-exponential fit of the transient kinetics displayed in the main graph of Figure 6 (solid) shows that the use of Deriphat 160-C for the extraction and purification of RCs yields a preparation that is characterized solely by the long-lived ~1−1.5 s process (see also Figure 7A). The addition of a second exponential component did not significantly improve the fit as judged by the reduced χ^2 and the distribution of residuals. Thus, the Q_B site is fully occupied in these RCs as taken directly from an affinity column. Unlike the LDAO-purified RCs, the addition of UQ_6 has no effect on the time scale of the charge recombination kinetics in this sample (Figure 6, open symbols). It is likely that the small reduction in amplitude is due to the loss of some RC activity during the treatment that utilizes large amounts of detergent and heating to 28 °C during quinone incorporation. Rates of $P^+Q_B^-$ recombination in Deriphat- or LDAO-purified wild-type RCs ranged from 1.3 to 1.5 s—well within the bounds of previously published values (reviewed in refs *9* and *67*). While it has been shown that the rate of $P^+Q_A^-$ charge recombination can vary because of detergent-induced changes in the electronic structure of P (*51*, *65*, *66*), this was not observed here (Table 2). We also note that the difference in the position of the near-infrared band of P (Figure 5) has not affected the $P^+Q_B^-$ charge recombination rate constant.

Terbutryn Titration. Assignment of transient kinetics to the formation or recombination of $P^+Q_B^-$ is validated by a demonstration that these signals disappear with the addition of a competitive inhibitor of Q_B binding (e.g., terbutryn). Deriphat-isolated wild-type RCs containing fully occupied Q_B sites were titrated with increasing amounts of terbutryn to determine the concentration necessary for complete inhibition of $P^+Q_B^-$ formation in a sample having no exogenous quinones. As is shown in Figure 4, ~90% of the P^+Q^- signal decays on the ms time scale with the addition of 50 μM terbutryn (~2.5 equiv). Complete inhibition of $P^+Q_B^-$ formation is achieved with 500 μM terbutryn (25 equiv), and this concentration was used for subsequent experiments. This amount of terbutryn was also effective at inhibiting samples to which UQ_6 had been added previously (not shown). Rates of $P^+Q_A^-$ recombination recorded after the addition of terbutryn to the wild-type and YFH RCs were similar to those reported in the literature (roughly 100 ms; Table 2, Figure 4 inset, Figure 7B,D).

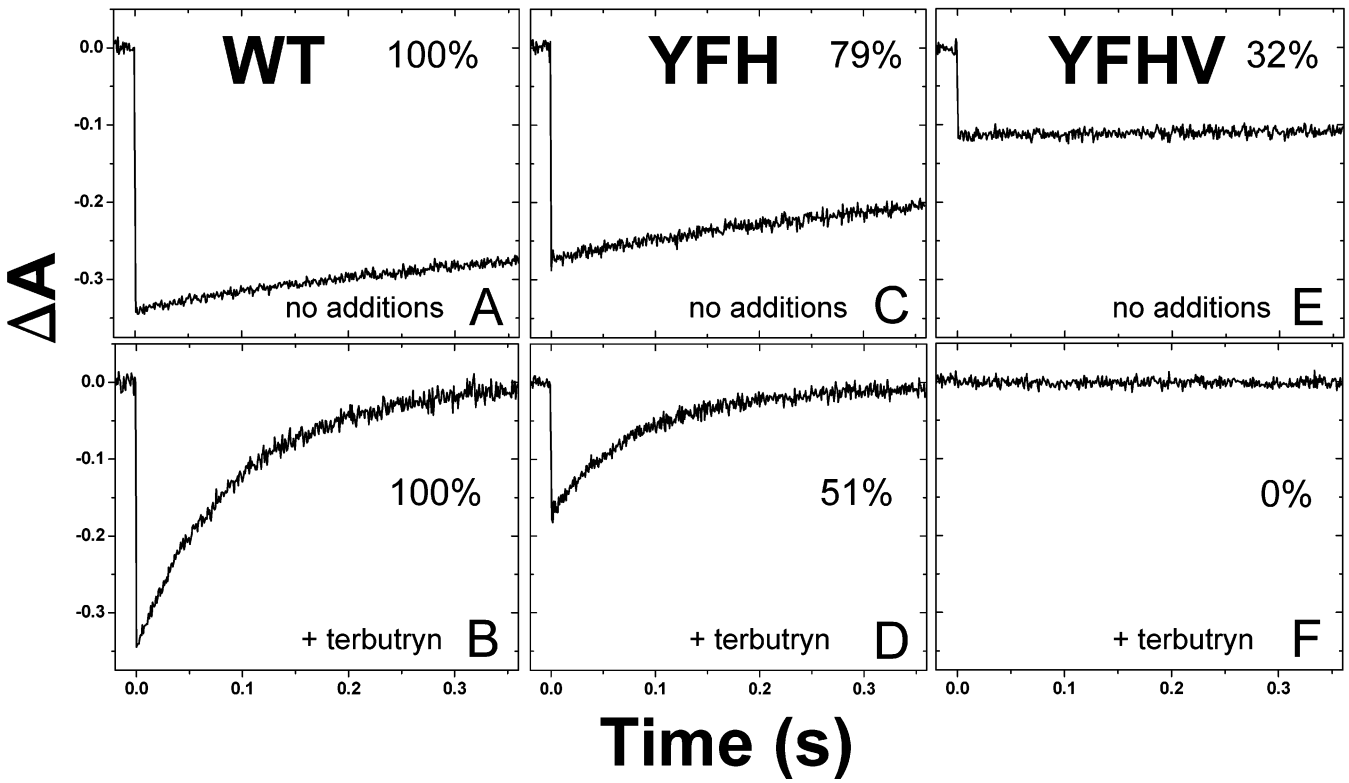

FIGURE 7: Kinetic profiles and yields of P^+Q^- states in Deriphat-purified wild-type (A and B), YFH mutant (C and D), and YFHV mutant (E and F) RCs of *R. capsulatus*. The concentration of RCs was ~20 μM. The amplitudes of the signals observed for the mutant RC samples ± inhibitor include contributions from a number of factors, as discussed in the text.

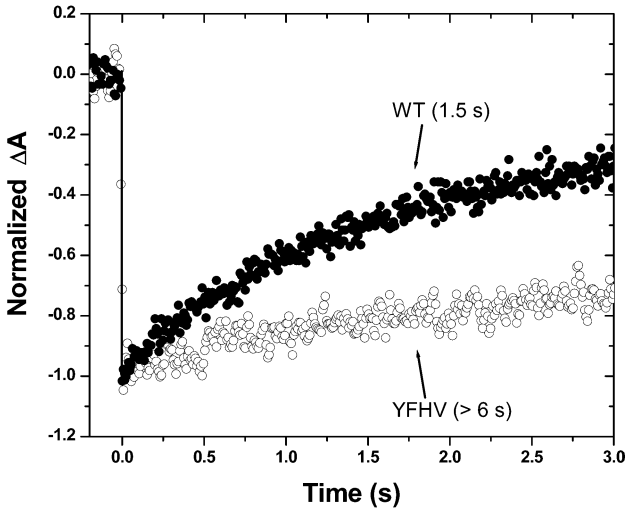

FIGURE 8: Kinetic profiles of recombination of long-lived $P^+Q_B^-$ states in the wild-type (solid circles) and YFHV mutant (open circles) *R. capsulatus* RCs.

Identification and Assignment of Transients. In native RCs of *R. capsulatus*, decay of $P^+Q_B^-$ by charge recombination normally proceeds via an indirect pathway that involves $P^+Q_A^-$ ($k_{Q_BP,i}$; Figure 1)—a state with which it is in equilibrium—followed by activationless decay of $P^+Q_A^-$ to the ground state (k_{Q_AP}; refs *68* and *69*). An alternative, direct route of $P^+Q_B^-$ charge recombination ($k_{Q_BP,d}$; Figure 1), which involves electron transfer through the B-side protein matrix, predominates when the free energy gap between the $P^+Q_B^-$ and $P^+Q_A^-$ states is increased by, for example, mutagenesis, low pH, or quinone substitution (*68*, *70*−*73*). The rate of the $P^+Q_B^- \rightarrow PQ_B$ reaction occurring via the direct route has been shown to be at least 5−10 times slower than that of the indirect route; this rate ($k_{Q_BP,d}$) varies with pH from ∼10 s^{-1} at pH 6.0 to ∼4 s^{-1} at pH 10.0, as does the amount of the $P^+Q_B^-$ state that decays via this mechanism (*71*). The direct route is the dominant pathway for charge recombination in site-specific mutants in which the free energy of the $P^+Q_B^-$ charge-separated state has been lowered by several tens of meV (*70*, *72*), or the free energy of $P^+Q_A^-$ has been raised by a comparable amount (*73*).

We now discuss more fully the results obtained with Deriphat-purified mutant RC samples taken directly from column chromatography (see Figure 4). The Q_B sites in these RCs remain fully occupied. For the reasons delineated above, the fact that $P^+Q_B^-$ charge recombination kinetics can be measured without quinone reconstitution is of significant utility to this study; it is probably even more important for ultrafast experiments that monitor directly the $H_B^- \rightarrow Q_B$ electron-transfer reaction in the same RC samples (*59*).

The YFHV mutant RCs showed a sustained P bleach of extremely long duration (Figure 7E) that is lost with the addition of terbutryn (Figure 7F) or stigmatellin (not shown). The decay time of this transient is significantly longer than that observed for a similar state in the wild-type RC (Figure 8). Thus, we assign this long-lived signal in the YFHV mutant RC to $P^+Q_B^-$ formed through the B-side electron-transfer cofactors (Figure 1) based upon its long-lived nature (>6 s) and its disappearance in the presence of inhibitors. If $P^+Q_B^-$ had been formed from $P^+Q_A^-$ in the YFHV mutant RC (e.g., if the M250V substitution had not quantitatively blocked Q_A binding), then the latter state would also have been available for the indirect decay pathway of $P^+Q_B^-$, affording a charge recombination time of 1.3−1.5 s, as was seen in the wild-type RC (Figure 7A); instead, we observe a $P^+Q_B^-$ lifetime of >6 s, more in keeping with a direct pathway not involving (and not requiring the presence of) Q_A. Furthermore, if electrons were transferred to Q_B from Q_A^- in these mutant RCs (e.g., again if some Q_A were present despite the M250V substitution), then addition of an inhibitor of Q_B binding should have resulted in a short-lived (∼100 ms) $P^+Q_A^-$ charge recombination signal as is observed in the control RCs (Figure 7B,D). In contrast to the transients observed in wild-type and YFH mutant RCs, no short-lived (s or ms) signals are observed in the YFHV RC upon addition of inhibitor, as is emphasized by the time scale of the data presented in Figure 7. Thus, no transient signals assignable either directly to $P^+Q_A^-$ or to the involvement of this state in the formation or decay of $P^+Q_B^-$ are observed in RCs harboring the W(M250)V substitution.

The most complicated kinetics that we observed belong to the Q_B-occupied RC of the YFH mutant. The kinetics from the YFH RC are biphasic with lifetimes of ∼1 s (60%) and ∼6−10 s (40%). YFH mutant RCs are capable of transferring electrons to Q_B via both the A and B branches of cofactors; thus, the sole, long-lived (>6 s) signal observed in YFHV RCs (where Q_A is absent) must also be a part of the time profile in the YFH mutant RCs. On this basis, we assign the phase with a lifetime of 6−10 s to direct charge recombination of $P^+Q_B^-$ ($k_{Q_BP,d}$) in the population of YFH RCs in which this state formed via the B-side pathway. Since its time constant matches that seen in the wild-type RCs, the phase with a lifetime of ∼1 s is then assigned to indirect charge recombination of $P^+Q_B^-$ ($k_{Q_BP,i}$) in the population of RCs in which this state formed via the A-side pathway. These assignments require the RCs to have "memory" as to the path by which the state was formed. We thus have strong evidence that $P^+Q_B^-$ formed via B-side electron-transfer recombines without involving the $P^+Q_A^-$ intermediate even though the latter state (as well as Q_A) is present. Conversely, $P^+Q_B^-$ formed via the A-pathway recombines more rapidly using the indirect pathway (Figure 1). Other interpretations are rendered less likely based on the combination and consistency of (1) the recombination kinetics described above, (2) the relative amplitudes of the associated P^+Q^- signals (vide infra), and (3) the branching ratios for the decay routes of P* and intermediates forming the P^+Q^- states (from fs studies on the same RCs, ref *59*).

Complex $P^+Q_B^-$ decays are commonly seen in wild-type RCs (*74*−*76*) and indicate heterogeneities in structural and energetic factors that influence the rate of the indirect charge recombination reaction. The direct route for $P^+Q_B^-$ charge recombination predominates in wild-type RCs under conditions of low pH and in mutant RCs in which $P^+Q_B^-$ is modestly lowered in free energy relative to $P^+Q_A^-$ (*70*, *72*). In the YFH RC studied here, it seems likely on the basis of the two distinct kinetic components that two phases indeed reflect utilization of both the indirect and the direct routes that relate to different properties of $P^+Q_B^-$ formed via the two branches. Following this logic, for the population of YFH RCs in which $P^+Q_B^-$ forms via the B branch, this state may lie sufficiently far below $P^+Q_A^-$ in free energy that the indirect route is inoperable. The conclusion that $P^+Q_B^-$ formed via the B branch does not utilize $P^+Q_A^-$ for

recombination—although $P^+Q_B^-$ produced from the A branch does—can be potentially understood on energetic grounds, but structural aspects may also apply.

This situation could be achieved by relaxation events (such as conformational changes, proton uptake, etc.) that can occur during reduction of Q_A, during $Q_A^- \rightarrow Q_B$ electron transfer, or after this reaction. These processes may stabilize $P^+Q_A^-$ and/or destabilize $P^+Q_B^-$ so the two states are rendered sufficiently close in free energy for the indirect pathway for $P^+Q_B^-$ charge recombination to function. In this scenario, such relaxations would not occur (or a different set of relaxations may occur) if $P^+Q_B^-$ forms from the B branch instead, leaving this state sufficiently below $P^+Q_A^-$ so that only the direct pathway (not using the $P^+Q_A^-$ state) would be operable. Similarly, processes occurring upon formation of $P^+Q_B^-$ by either branch may have structural consequences influencing the distance between Q_A and Q_B^- and thus the rate of the indirect route. It should be noted that conformational changes and protonation events accompanying the formation and decay of the P^+Q^- states in the RC have been observed and discussed (e.g., refs *7*, *8*, and *77*−*84*), and some of these may contribute to the new observations that we have made here on the YFH RC. We will briefly return to this issue in the concluding remarks.

Estimated Yield of the $H_B^- \rightarrow Q_B$ Electron-Transfer Reaction. Forward electron transfer processes are extremely efficient in wild-type RCs. Initial charge separation reactions that aggressively separate positive and negative charges across a distance that spans 30 Å sacrifice energy for rate and quantum yield. At every branched step, the rate constant for forward electron transfer exceeds the rate constant for charge recombination by at least an order of magnitude. The yields of P^+Q^- states in wild-type RCs approach unity (*5*); thus, we have assumed the yield of $P^+Q_A^-$ and $P^+Q_B^-$ in wild-type RCs to be 100% in this study (Figure 7A).

Qualification of Estimated Yields. While we report estimated yields below, exhaustive comparison of the yields of $P^+Q_B^-$ formed in the mutant RCs is not possible because of the potential for variable amounts of sample recycling that may occur during the ∼7-ns FWHM excitation flashes. Many decay processes within a mutant RC return the complex to its ground state such that it can receive a second excitation within the duration of the laser pulse. Of primary concern for YFH and YFHV mutant RCs is the rapid deactivation process (Figure 2) whereby P* can return directly to the ground state in 100−200 ps (*26*, *59*). In addition, charge recombination of $P^+\beta^-$ or $P^+H_B^-$ (k_{H_BP}; Figure 1) on the ns time scale also contributes to recycling. The result is that long-lived states such as $P^+Q_B^-$ accumulate to a higher population than is reflective of the true quantum yield that would be obtained during a single turnover of the RC. Nonetheless, we can derive useful estimates for the yield of $P^+Q_B^-$ from these measurements for later comparison with the values obtained in fs studies on the same RC samples that directly probe the $H_B^- \rightarrow Q_B$ process (*59*).

Estimated Yields of $P^+Q_B^-$ Formed by B-Branch Electron Transfer in YFHV RCs. To assay secondary, forward electron transfer, we compared directly the amplitude of P bleaching associated with $P^+Q_B^-$ in the wild-type RC to that observed in the YFHV mutant RC. Our specific interest was the efficiency of forward electron transfer from $P^+H_B^-$. In Deriphat-purified YFHV RCs, we observed long-lived signals with amplitudes of ∼30% of that of the wild type (Figures 7A,C). This amount of $P^+Q_B^-$ (formed solely via the B branch) can be compared to the yield of 30−35% for $P^+H_B^-$ determined by ultrafast spectroscopy with LDAO-purified YFH RCs (*26*) and Deriphat-purified YFHV RCs (*59*) to obtain an estimate of ∼85−100% for the yield of $H_B^- \rightarrow Q_B$ electron transfer. As discussed above, this value for YFHV mutant RC is likely to be high because of significant recycling.

P^+Q^- Formation in YFH Mutant RCs. In the YFH RC, $P^+Q_B^-$ forms via both A- and B-side electron-transfer pathways (Figure 3B), with consequent biphasic recombination kinetics (vide supra) having respective relative contributions of 0.6 (∼1 s phase) and 0.4 (6−10 s phase). The A side still functions when Q_B is inhibited with terbutryn and gives the transient signal expected for $P^+Q_A^-$ charge recombination (vide supra). These changes in the kinetics of the recovery of the 860-nm P bleach upon the addition of terbutryn to Deriphat-purified YFH RCs taken directly off the affinity column are accompanied by a dramatic, but expected, reduction in the amplitude of P^+Q^- signals (compare Figures 7C,D). In assessing this signal reduction, we note that the amplitude without terbutryn (79% of the signal from wild-type RCs) and with terbutryn (51% of the signal from wild-type RCs) are both governed by the interplay of the competing decay routes of P* and of the A- and B-side intermediates ($P^+\beta^-$ and $P^+H_B^-$) in giving $P^+Q_A^-$ and $P^+Q_B^-$ (delineated in ref *59*) plus partial recycling through these shorter-lived states. The latter effect is common to the two samples (YFH RCs ± terbutryn), so that the 28% drop in amplitude seen in YFH RCs with inhibitor can be attributed to the loss of $P^+Q_B^-$ formed via the B pathway. This value is in good agreement with the B-branch yield of $P^+Q_B^-$ of 32% estimated above of the YFHV RC.

We note that there is internal consistency in the signal amplitudes/yields associated with the various processes in the set of samples: (1) The amplitude of the signal observed in YFHV RCs (32% of the signal seen in wild-type RCs) equals the amplitude of the slow phase observed in terbutryn-treated YFH RCs ($0.4 \times 79\% = 32\%$), both reflecting $P^+Q_B^-$ decay by the direct route; (2) the amplitude lost by addition of terbutryn to YFHV RCs (32%) is approximately equal to the amplitude lost by addition of terbutryn to YFH RCs (28%), both reflecting $P^+Q_B^-$ formed solely via the B branch; and (3) the amplitude of the fast phase in YFH RCs ($0.6 \times 79\% = 48\%$) is comparable to the amplitude of the only phase observed in terbutryn-inhibited YFH RCs (51%).

Because of recycling, the 28% yield of $P^+Q_B^-$ for the YFH RC, like the similar value for YFHV RC, must be considered an overestimate. However, taken at face value, a 28% yield as compared with a quantum yield of 30−35% for $P^+Q_B^-$ obtained from the ultrafast measurements on the LDAO-purified YFH RC (*26*) and Deriphat-purified YFH and YFHV mutant RCs (*59*) would suggest an average $P^+H_B^- \rightarrow P^+Q_B^-$ yield of 85%. Such a value is at the upper end of the 50 ± 30% range obtained from the ultrafast studies (*59*), which is in good agreement considering that the value from the ultraslow measurements is an overestimate and taking into account the associated error in the yield from the ultrafast study.

Although recycling during the relatively long ∼7-ns excitation flashes used for the present study limits our ability

to draw firm quantitative conclusions on the $P^+Q_B^-$ yield from these studies alone, these experiments were designed taking this limitation into account. We established conditions to (1) provide signals of sufficiently high amplitude and quality for kinetic analysis and for accurately probing the affects of inhibitors, and (2) utilize identical sample conditions (concentrations, path length, etc.) involving the new mutant RCs and fully Q_B-occupied RCs that would be used for ultrafast measurements (where the $P^+H_B^- \rightarrow P^+Q_B^-$ reaction is directly probed). The aim of the ultraslow studies reported here was to demonstrate unequivocally that $P^+Q_B^-$ forms from B-branch transfer, and the results described above show that this goal has been achieved successfully. It should be noted that ultraslow measurements can be designed to minimize recycling complications by using 30-ps excitation flashes (for example), although such measurements can suffer a degradation in signal amplitudes and averaging capabilities because of laser characteristics (energy, stability, and repetition rate). We have previously carried out such measurements and found lower apparent yields of $P^+Q_B^-$ formed via B-branch cofactors in mutant RCs than were obtained using the longer flashes (*30*). However, these experiments utilized a different series of mutant RCs than that studied here, and the samples were purified with LDAO and, thus, required Q_B reconstitution, with all the attendant complications (*7*). In those previous studies, we found that mutant RCs with a native Q_B binding pocket gave an estimated yield of 60−70% for electron transfer from H_B^- to Q_B, and the yield of this reaction appeared to increase substantially after mutagenic modification of the Q_B binding pocket to lower the free energy of $P^+Q_B^-$ (*30*).

Rate of $H_B^- \rightarrow Q_B$ Electron Transfer. For the purpose of discussion, if we combine a yield for electron transfer from H_B^- to Q_B of ∼85% from the ultraslow amplitude data described above (known to be an overestimate) or a mean value of ∼50% from the ultrafast measurements to be reported shortly (*59*) along with a reasonable $P^+H_B^-$ charge recombination time constant of 1−10 ns (k_{H_BP}), then the time constant for $P^+H_B^- \rightarrow P^+Q_B^-$ is likely on the order of several ns. These considerations suggest that B-branch electron transfer from H_B^- to Q_B is significantly slower than the corresponding A-branch electron transfer from H_A^- to Q_A, which occurs in ∼200 ps. Although there are many possible contributions to potential differences in rates of secondary electron transfer on the two branches, one difference is that the B branch does not feature a Trp residue positioned between H_B and Q_B; the symmetry-related counterpart to M250Trp on the A side is L216Phe on the B side. In RCs of both *R. capsulatus* (*61*) and *R. sphaeroides* (*63*), replacement of A-side residue M250Trp with Phe (M252 in *R. sphaeroides*) slowed the rate of $H_A^- \rightarrow Q_A$ electron transfer 4−5-fold to ∼0.9 ns^{-1}. Thus, the absence of a Trp between H_B and Q_B may make a significant contribution to the slow $H_B^- \rightarrow Q_B$ electron transfer. We have attempted to probe this effect directly by substituting a Trp for the native Phe at L216, but further analysis is required to sort out issues that have arisen[2].

Structural and Energetic Factors Influencing Activity of the Quinones. Much speculation has been made recently of the functional significance of variable binding sites for Q_B that are observed in the structures of wild-type and mutant RCs (*4*, *85*−*88*). The position of Q_B is most dramatically different in the structures of wild-type RCs that were derived from crystals that were frozen under continuous illumination (light structure) versus crystals that were frozen in the dark (dark structure; refs *85* and *88*). In the light structure, Q_B is located in a position that is proximal to the iron−ligand complex, closest to Q_A. In the structure that was obtained from crystals frozen in the dark, Q_B is bound in a position that is more distal to Q_A and the iron−ligand complex. The $Q_A^- \rightarrow Q_B$ electron-transfer reaction ($k_{Q_AQ_B}$; Figure 1) is independent of driving force and is known to be conformationally gated (*89*−*91*)—when RCs are in the optimal conformation, forward electron transfer occurs at a more rapid rate than it does in RCs that are in a sub-optimal conformation. In native RCs, the formation of $P^+Q_A^-$ is the trigger that induces these conformational changes to set the RC for rapid delivery of the electron to Q_B. Subsequent proton uptake events further stabilize the $P^+Q_B^-$ state such that its lifetime is at least 10-fold longer than that of the $P^+Q_A^-$ intermediate (reviewed in refs *9*, *10*, and *80*).

Movement of Q_B into the proximal site was suggested to represent at least a portion of the conformational change that allows rapid forward electron transfer from Q_A^- to Q_B (*85*, *88*), but other evidence says proton uptake is involved (*83*, *84*). We note that formation of $P^+Q_B^-$ in the YFHV RC occurs in the absence of any events that are initiated by formation of the $P^+Q_A^-$ state since Q_A is quantitatively absent in this mutant RC. The driving forces for formation of $P^+Q_B^-$ via the two pathways are expected to be quite different. If electron transfer from H_B^- to Q_B can be viewed as being analogous to A-side formation of the $P^+Q_A^-$ state, this B-side reaction should be thermodynamically favorable. Thus, the conformational gating or energetic relaxation events that are known to accompany and enable formation of $P^+Q_B^-$ via the A-side pathway may not be needed.

Our data cannot say where the quinone is located within the Q_B binding pocket of the YFH or YFHV RCs. Mutations near the quinones have been shown to affect the binding site preference of Q_B (*87*, *92*). In fact, Q_B occupies the proximal site in the structure of an *R. sphaeroides* RC carrying the M260Ala → Trp substitution in the Q_A site; thus, in lieu of a structure we cannot predict the effect of the W(M250)V mutation (near Q_A) on the position of Q_B in the YFHV RC. We note that if any movement of Q_B into a proper site is required for the $H_B^- \rightarrow Q_B$ electron-transfer reaction, it occurs on a time scale that is more rapid than that of the ns electron transfer.

[2] In an effort to determine whether the reduced efficiency of forward, secondary electron transfer on the B side is associated with the presence of a Phe instead of a Trp at L216, we have constructed the F(L216)W mutation and have linked it to the YFHV mutations to yield the YWFHV mutant RC. Although analysis of the behavior of this RC is still underway, preliminary ultraslow measurements report kinetics identical to that of YFHV with reduced amplitude (data not shown). We suspect that the smaller signals are a result of nonquantitative occupancy of the Q_B site and are using the singly mutated F(L216)W RC to determine the effects of the Trp substitution on Q_B binding. Until the effects are understood, we cannot comment further on the effect of the Trp at L216 on the rate of electron transfer from H_B^- to Q_B. However, we can state that the rate of recombination of $P^+Q_B^-$ formed in the YWFHV RC appears to be unchanged from that of the YFHV RC (data not shown). This latter result indicates that the Trp substitution at L216 does not alter the route for charge recombination of $P^+Q_B^-$ in this RC.

Highly relevant to these issues are our findings on the YFH RC indicating the possibility that $P^+Q_B^-$ formed via the A branch utilizes that branch for the indirect (~1 s) decay pathway, whereas $P^+Q_B^-$ formed via the B branch decays primarily or exclusively by the direct (6−10 s) route. This memory that $P^+Q_B^-$ displays in using a decay route that is interrelated to its formation pathway may very well reflect the involvement of events occurring within the protein matrix on various time scales that may be significant for one pathway but not the other. In essence, the key question raised by these considerations is whether the $P^+Q_B^-$ state formed via the B branch is the same $P^+Q_B^-$ state formed via the A branch in terms of the features of the protein environment that contribute to factors (free energies, electronic couplings, reorganization energies) that determine the rates of the various P^+Q^- processes (electron transfer, proton uptake, etc.). The results obtained here on the YFH and YFHV mutant RCs give tantalizing hints that the $P^+Q_B^-$ states formed via the two branches are not precisely the same, as reflected by the different charge recombination kinetics. These differences may be reporting to some extent on the functionally significant protein response events that occur upon the formation and decay of $P^+Q_A^-$ by the normal A-branch pathway and subsequent events that occur following $P^+Q_A^- \rightarrow P^+Q_B^-$ electron transfer. Future studies comparing the properties of $P^+Q_B^-$ (and possibly $P^+Q_B^=$) formed via one or both branches using the same or related mutants and the protocols developed here should help to answer the questions posed above and open up new opportunities for exploring structure/function relationships that modulate the activity of the P^+Q^- states.

ACKNOWLEDGMENT

We thank David Tiede for insightful comments on the manuscript.

REFERENCES

1. Deisenhofer, J., Epp, O., Miki, K., Huber, R., and Michel, H. (1985) Structure of the protein subunits in the photosynthetic reaction center from *Rhodopseudomonas viridis* at 3 Å resolution, *Nature 318*, 618−624.
2. Allen, J. P., Feher, G., Yeates, T. O., Komiya, H., and Rees, D. C. (1987) Structure of the reaction center from *Rhodobacter sphaeroides* R-26: The cofactors, *Proc. Natl. Acad. Sci. U.S.A. 84*, 5730−5734.
3. Chang, C.-H., El-Kabbani, O., Tiede, D. M., Norris, J. R., and Schiffer, M. (1991) The structure of the membrane-bound photosynthetic reaction center from *Rhodobacter sphaeroides*, *Biochemistry 30*, 5352−5360.
4. Ermler, U., Fritsch, G., Buchanan, S. K., and Michel, H. (1994) Structure of the photosynthetic reaction centre from *Rhodobacter sphaeroides* at 2.65 Å resolution: cofactor and protein−cofactor interactions, *Structure 2*, 925−936.
5. Woodbury, N. W., and Allen, J. P. (1995) The pathway, kinetics, and thermodynamics of electron transfer in wild type and mutant reaction centers of purple nonsulfur bacteria, In *Anoxygenic Photosynthetic Bacteria* (Blankenship, R. E., Madigan, M. T., and Bauer, C. E., Eds.) pp 527−557, Kluwer, The Netherlands.
6. Leibl, W., and Breton, J. (1991) Kinetic properties of the acceptor quinone complex in *Rhodopseudomonas viridis*, *Biochemistry 30*, 9634−9642.
7. Tiede, D. M., Vazquez, J., Cordova, and Marone, P. A. (1996) Time-resolved electrochromism associated with the formation of quinone anions in the *Rhodobacter sphaeroides* R-26 reaction center, *Biochemistry 35*, 10763−10775.
8. Li, J., Gilroy, D., Tiede, D. M., and Gunner, M. R. (1998) Kinetic phases in the electron transfer from P^+Q_A-Q_B to $P^+Q_AQ_B$- and the associated processes in *Rhodobacter sphaeroides* R-26 reaction centers, *Biochemistry 37*, 2818−2829.
9. Sebban, P., Maróti, P., and Hanson, D. K. (1995) Electron and proton-transfer to the quinones in bacterial photosynthetic reaction centers−insight from combined approaches of molecular genetics and biophysics, *Biochimie 77*, 677−694.
10. Okamura, M. Y., and Feher, G. (1995) Proton-coupled electron-transfer reactions of Q_B in reaction centers from photosynthetic bacteria, In *Anoxygenic Photosynthetic Bacteria* (Blankenship, R. E., Madigan, M. T., and Bauer, C. E., Eds.) pp 577−594, Kluwer, Dordrecht, The Netherlands.
11. Kirmaier, C., and Holten, D. (1987) Primary photochemistry of reaction centers from the photosynthetic purple bacteria, *Photosyn. Res. 13*, 225−260.
12. Michel-Beyerle, M. E., Plato, M., Deisenhofer, J., Michel, H., Bixon, M., and Jortner, J. (1988) Unidirectionality of charge separation in reaction centers of photosynthetic bacteria, *Biochim. Biophys. Acta 932*, 52−70.
13. Plato, M., Mobius, K., Michel-Beyerle, M. E., Bixon, M., and Jortner, J. (1988) Intermolecular electronic interactions in bacterial photosynthesis, *J. Am. Chem. Soc. 110*, 7279−7285.
14. Kellogg, E. C., Kolaczkowski, S., Wasielewski, M. R., and Tiede, D. M. (1989) Measurement of the extent of electron transfer to the bacteriopheophytin in the M-subunit in reaction centers of *Rhodopseudomonas viridis*, *Photosyn. Res. 22*, 47−59.
15. Scherer, P. O. J., and Fischer, S. F. (1989) Quantum treatment of the optical spectra and the initial electron-transfer process within the reaction center of *Rhodopseudomonas viridis*, *Chem. Phys. 131*, 115−127.
16. Parson, W. W., Chu, Z.-T., and Warshel, A. (1990) Electrostatic control of charge separation in bacterial photosynthesis, *Biochim. Biophys. Acta 1017*, 251−272.
17. Steffen, M. A., Lao, K., and Boxer, S. G. (1994) Dielectric asymmetry in the photosynthetic reaction center, *Science 264*, 810−816.
18. Heller, B. A., Holten, D., and Kirmaier, C. (1995) Control of electron transfer between the L- and M-sides of photosynthetic reaction centers, *Science 269*, 940−945.
19. Alden, R. G., Parson, W. W., Chu, Z. T., and Warshel, A. (1995) Calculations of electrostatic energies in photosynthetic reaction centers, *J. Am. Chem. Soc. 117*, 12284−12298.
20. Gunner, M. R., Nicholls, A., and Honig, B. (1996) Electrostatic potentials in *Rhodopseudomonas viridis* reaction centers: implications for the driving force and directionality of electron transfer, *J. Phys. Chem. 100*, 4277−4291.
21. Ivashin, N., Kallebring, B., Larsson, S., and Hansson, O. (1998) Charge separation in photosynthetic reaction centers, *J. Phys. Chem. B 102*, 5017−5022.
22. Zhang, L. Y., and Friesner, R. A. (1998) Ab initio calculation of electronic coupling in the photosynthetic reaction center, *Proc. Natl. Acad. Sci. U.S.A. 95*, 13603−13605.
23. Hasegawa, J., Ohkawa, K., and Nakatsuji, H. (1998) Excited states of the photosynthetic reaction center of *Rhodopseudomonas viridis*: SAC-CI study, *J. Phys. Chem. B 102*, 10410−10419.
24. Katilius, E., Turanchik, T., Lin, S., Taguchi, A. K. W., and Woodbury, N. W. (1999) B-side electron transfer in a *Rhodobacter sphaeroides* reaction center mutant in which the B-side monomer bacteriochlorophyll is replaced with bacteriopheophytin, *J. Phys. Chem. B 103*, 7386-7389.
25. Kolbasov, D., and Scherz, A. (2000) Asymmetric electron transfer in reaction centers of purple bacteria strongly depends on different electron matrix elements in the active and inactive branches, *J. Phys. Chem. B 104*, 1802−1809.
26. Kirmaier, C., He, C., and Holten, D. (2001) Manipulating the direction of electron transfer in the bacterial reaction center by swapping Phe for Tyr near BChl(M) (L181) and Tyr for Phe near BChl(L) (M208), *Biochemistry 40*, 12132−12139.
27. Pincak, R., and Pudlak, M. (2001) Noise breaking the 2-fold symmetry of photosynthetic reaction centers: Electron transfer, *Phys. Rev. E 64*, 031906.
28. Lin, S., Jackson, J. A., Taguchi, A. K. W., and Woodbury, N. W. (1999) B-side electron-transfer promoted by absorbance of multiple photons in *Rhodobacter sphaeroides* R-26 reaction centers, *J. Phys. Chem. B 103*, 4757−4763.
29. Lin, S., Katilius, E., Haffa, A. L., Taguchi, A. K., and Woodbury, N. W. (2001) Blue light drives B-side electron transfer in bacterial photosynthetic reaction centers, *Biochemistry 40*, 13767−13773.
30. Laible, P. D., Kirmaier, C. K., Holten, D., Tiede, D. M., Schiffer, M., and Hanson, D. K. (1998) Formation of $P^+Q_B^-$ via B-branch

electron transfer in mutant reaction centers, In *Photosynthesis: Mechanisms and Effects* (Garab, G., Ed.) pp 849−852, Kluwer, Dordrecht, The Netherlands.
31. Kirmaier, C., Weems, D., and Holten, D. (1999) M-side electron transfer in reaction center mutants with a lysine near the nonphotoactive bacteriochlorophyll, *Biochemistry 38*, 11516−11530.
32. Katilius, E., Katiliene, Z., Lin, S., Taguchi, A. K. W., and Woodbury, N. W. (2002) B-side electron transfer in a *Rhodobacter sphaeroides* reaction center mutant in which the B side monomer bacteriochlorophyll is replaced with bacteriopheophytin: Low temperature study and energetics of charge-separated states, *J. Phys. Chem. B 106*, 1471−1475.
33. Kirmaier, C., Laible, P. D., Czarnecki, K., Hata, A. N., Hanson, D. K., Bocian, D. F., and Holten, D. (2002) Comparison of M-side electron transfer in *R. sphaeroides* and *R. capsulatus* reaction centers, *J. Phys. Chem. B 106*, 1799−1808.
34. de Boer, A. L., Neerken, S., de Wijn, R., Permentier, H. P., Gast, P., Vijgenboom, E., and Hoff, A. J. (2002) High yield of B-branch electron transfer in a quadruple reaction center mutant of the photosynthetic bacterium *Rhodobacter sphaeroides*, *Biochemistry 41*, 3081−3088.
35. de Boer, A. L., Neerken, S., de Wijn, R., Permentier, H. P., Gast, P., Vijgenboom, E., and Hoff, A. J. (2002) B-branch electron transfer in reaction centers of *Rhodobacter sphaeroides* assessed with site-directed mutagenesis, *Photosyn. Res. 71*, 221−239.
36. Nagarajan, V., Parson, W. W., Gaul, D., and Schenck, C. (1990) Effect of specific mutations of tyrosine-(M)210 on the primary photosynthetic electron-transfer process in *Rhodobacter sphaeroides*, *Proc. Natl. Acad. Sci. U.S.A. 87*, 7888−7892.
37. Finkele, U., Lauterwasser, C., Zinth, W., Gray, K. A., and Oesterhelt, D. (1990) Role of tyrosine M210 in the initial charge separation of reaction centers of *Rhodobacter sphaeroides*, *Biochemistry 29*, 8517−8521.
38. Chan, C.-K., Chen, L. X.-Q., DiMagno, T. J., Hanson, D. K., Nance, S. L., Schiffer, M., Norris, J. R., and Fleming, G. R. (1991) Initial electron transfer in photosynthetic reaction centers of *Rhodobacter capsulatus* mutants, *Chem. Phys. Lett. 176*, 366−372.
39. Du, M., Rosenthal, S. J., Xie, X., DiMagno, T. J., Schmidt, M., Hanson, D. K., Schiffer, M., Norris, J. R., and Fleming, G. R. (1992) Femtosecond spontaneous-emission studies of reaction centers from photosynthetic bacteria, *Proc. Natl. Acad. Sci. U.S.A. 89*, 8517−8521.
40. Gray, K. A., Wachtveitl, J., and Oesterhelt, D. (1992) Photochemical trapping of a bacteriopheophytin anion in site-specific reaction-center mutants from the photosynthetic bacterium *Rhodobacter sphaeroides*, *Eur. J. Biochem. 207*, 723−731.
41. Jia, Y., DiMagno, T. J., Chan, C.-K., Wang, Z., Du, M., Hanson, D. K., Schiffer, M., Norris, J. R., Fleming, G. R., and Popov, M. S. (1993) Primary charge separation in mutant reaction centers of *Rhodobacter capsulatus*, *J. Phys. Chem. 97*, 13180−13191.
42. Nagarajan, V., Parson, W. W., Davis, D., and Schenck, C. C. (1993) Kinetics and free energy of electron-transfer reactions in *Rhodobacter sphaeroides* reaction centers, *Biochemistry 32*, 12324−12336.
43. Hamm, P., Gray, K. A., Oesterhelt, D., Feick, R., Scheer, H., and Zinth, W. (1993) Subpicosecond emission studies of bacterial reaction centers, *Biochim. Biophys. Acta 1142*, 99−105.
44. Alden, R. G., Parson, W. W., Chu, Z. T., and Warshel, A. (1996) Orientation of the OH dipole of tyrosine (M)210 and its effect on electrostatic energies in photosynthetic bacterial reaction centers, *J. Phys. Chem. 100*, 16761−16770.
45. Beekman, L. M. P., van Stokkum, I. H. M., Monshouwer, R., Rijnders, A. J., McGlynn, P., Visschers, R. W., Jones, M. R., and van Grondelle, R. (1996) Primary electron transfer in membrane-bound reaction centers with mutations at the M210 position, *J. Phys. Chem. 100*, 7256−7268.
46. Laible, P. D., Greenfield, S. R., Wasielewski, M. R., Hanson, D. K., and Pearlstein, R. M. (1997) Antenna excited-state decay kinetics establish primary electron transfer in reaction centers as heterogeneous, *Biochemistry 36*, 8677−8685.
47. DiMagno, T. J., Laible, P. D., Reddy, N. R., Small, G. J., Norris, J. R., Schiffer, M., and Hanson, D. K. (1998) Protein-chromophore interactions: spectral shifts report the consequences of mutations in the bacterial photosynthetic reaction center, *Spectrochim. Acta A54*, 1247−1267.
48. Streltsov, A. M., Vulto, S. I. E., Shkuropatov, A. Y., Hoff, A. J., Aartsma, T. J., and Shuvalov, V. A. (1998) B-A and B-B absorbance perturbations induced by coherent nuclear motions in reaction centers from *Rhodobacter sphaeroides* upon 30-fs excitation of the primary donor, *J. Phys. Chem. 102*, 7293−7298.
49. Zhou, H., and Boxer, S. G. (1998) Probing excited-state electron transfer by resonance Stark spectroscopy. 1. Experimental results for photosynthetic reaction centers, *J. Phys. Chem. 102*, 9139−9147.
50. Prince, R. C., and Youvan, D. C. (1987) Isolation and spectroscopic properties of photochemical reaction centers from *Rhodobacter capsulatus*, *Biochim. Biophys. Acta 890*, 286−291.
51. Wang, S., Lin, S., Woodbury, N. W., and Allen, J. P. (1994) Comparative study of reaction centers from purple photosynthetic bacteria: isolation and spectroscopy, *Photosyn. Res. 42*, 203-215.
52. Okamura, M. Y., Isaacson, R. A., and Feher, G. (1975) Primary acceptor in bacterial photosynthesis: obligatory role of ubiquinone in photoactive reaction centers of *Rhodopseudomonas spheroides*, *Proc. Natl. Acad. Sci. U.S.A. 72*, 3492−3495.
53. Gunner, M. R., and Dutton, P. L. (1989) ΔG dependence of the electron transfer from BPh^- to Q_A in reaction center protein from *Rhodobacter sphaeroides* with different quinones as Q_A, *J. Am. Chem. Soc. 111*, 3400−3412.
54. Bylina, E. J., Jovine, R. V. M., and Youvan, D. C. (1989) A genetic system for rapidly assessing herbicides that compete for the quinone binding site of photosynthetic reaction centers, *Bio/Technology 7*, 69−74.
55. Bylina, E. J., Robles, S. J., and Youvan, D. C. (1988) Directed mutations affecting the putative bacteriochlorophyll-binding sites in the light-harvesting I antenna of *Rhodobacter capsulatus*, *Isr. J. Chem. 28*, 73−78.
56. Simon, R., Priefer, U., and Puhler, A. (1983) A broad host range mobilization system for in vivo genetic engineering: Transposon mutagenesis in gram negative bacteria, *Bio/Technology 1*, 37−45.
57. Youvan, D. C., Ismail, S., and Bylina, E. J. (1985) Chromosomal deletion and plasmid complementation of the photosynthetic reaction center and light-harvesting genes from *Rhodopseudomonas capsulata*, *Gene 33*, 19−30.
58. Weaver, P. F., Wall, J. D., and Gest, H. (1975) Characterization of *Rhodopseudomonas capsulata*, *Arch. Microbiol. 105*, 207−216.
59. Kirmaier, C., Laible, P. D., Hanson, D. K., and Holten, D. (2003) B-side charge separation in bacterial photosynthetic reaction centers: Nanosecond time scale electron transfer from H_B^- to Q_B, *Biochemistry*, in press.
60. Plato, M., Michel-Beyerle, M. E., Bixon, M., and Jortner, J. (1989) On the role of tryptophan as a superexchange mediator for quinone reduction in photosynthetic reaction centers, *FEBS Lett. 249*, 70−74.
61. Coleman, W. J., Bylina, E. J., Aumeier, W., Siegl, J., Eberl, U., Heckmann, R., Ogrodnik, A., Michel-Beyerle, M. E., and Youvan, D. C. (1990) Influence of mutagenic replacements of tryptophan M250 on electron-transfer rates involving primary quinone in reaction centers of *Rhodobacter capsulatus*, In *Structure and Function of Bacterial Photosynthetic Reaction Centers* (Michel-Beyerle, M. E., Ed.) pp 273−281, Springer-Verlag, New York.
62. Stilz, H. Y., Finkele, U., Holzapfel, W., Lauterwasser, C., Zinth, W., and Oesterhelt, D. (1990) Site-directed mutagenesis of threonine M222 and tryptophan M252 in the photosynthetic reaction center of *Rhodobacter sphaeroides*, In *Structure and Function of Bacterial Photosynthetic Reaction Centers* (Michel-Beyerle, M. E., Ed.) pp 265−271, Springer-Verlag, New York.
63. Stilz, H. U., Finkele, U., Holzapfel, W., Lauterwasser, C., Zinth, W., and Oesterhelt, D. (1994) Influence of M subunit Thr222 and Trp252 on quinone binding and electron transfer in *Rhodobacter sphaeroides* reaction centres, *Eur. J. Biochem. 223*, 233−242.
64. Coleman, W. J., Bylina, E. J., and Youvan, D. C. (1990) Reconstitution of photochemical activity in *Rhodobacter capsulatus* reaction centers containing mutation at tryptophan M-250 in the primary quinone binding site, In *Current Research in Photosynthesis* (Baltscheffsky, M., Ed.) pp 149−152, Kluwer Academic Publishers, Dordrecht, The Netherlands.
65. Rautter, J., Lendzian, F., Lubitz, W., Wang, S., and Allen, J. P. (1994) Comparative study of reaction centers from photosynthetic purple bacteria: Electron paramagnetic resonance and electron nuclear double resonance spectroscopy, *Biochemistry 33*, 12077−12084.
66. Muh, F., Schulz, C., Schlodder, E., Jones, M. R., Rautter, J., Kuhn, M., and Lubitz, W. (1998) Effects of zwitterionic detergents on the electronic structure of the primary donor and the charge

recombination kinetics of P^+Q_A- in native and mutant reaction centers from *Rhodobacter sphaeroides*, *Photosyn. Res. 55*, 199−205.
67. Okamura, M. Y., Paddock, M. L., Graige, M. S., and Feher, G. (2000) Proton and electron transfer in bacterial reaction centers, *Biochim. Biophys. Acta 1458*, 148−163.
68. Kleinfeld, D., Okamura, M. Y., and Feher, G. (1984) Electron transfer in reaction centers of *Rhodopseudomonas sphaeroides*. I. Determination of the charge recombination pathway of $D^+Q_AQ_B^-$ and free energy and kinetic relations between $Q_A^-Q_B$ and $Q_AQ_B^-$, *Biochim. Biophys. Acta 766*, 126−140.
69. Woodbury, N. W., Parson, W. W., Gunner, M., Prince, R. A., and Dutton, P. L. (1986) Radical-pair energetics and decay mechanisms in reaction centers containing anthraquinones, naphthoquinones, or benzoquinones in place of ubiquinone, *Biochim. Biophys. Acta 851*, 16−22.
70. Takahashi, E., and Wraight, C. A. (1992) Proton and electron transfer in the acceptor quinone complex of *Rb. sphaeroides*: Characterization of site-directed mutants of the two ionizable residues, GluL212 and AspL213, in the Q_B binding site, *Biochemistry 31*, 855−866.
71. Labahn, A., Paddock, M. L., McPherson, P. H., Okamura, M. Y., and Feher, G. (1994) Direct charge recombination from $D^+Q_AQ_B^-$ to DQ_AQ_B in bacterial reaction centers from *Rhodobacter sphaeroides*, *J. Phys. Chem. 98*, 3417−3423.
72. Labahn, A., Bruce, J. M., Okamura, M. Y., and Feher, G. (1995) Direct charge recombination from $D^+Q_AQ_B^-$ to DQ_AQ_B in bacterial reaction centers from *Rhodobacter sphaeroides* containing low potential quinone in the Q_A site, *Chem. Phys. 197*, 355−366.
73. Allen, J. P., Williams, J. C., Graige, M. S., Paddock, M. L., Labahn, A., Feher, G., and Okamura, M. Y. (1998) Free energy dependence of the direct charge recombination from primary and secondary quinones in reaction centers from *Rhodobacter sphaeroides*, *Photosyn. Res. 55*, 227−233.
74. Gao, J.-L., Shopes, R. J., and Wraight, C. A. (1991) Heterogeneity of kinetics and electron-transfer equilibria in the bacteriopheophytin and quinone electron acceptors of reaction centers from *Rhodopseudomonas viridis*, *Biochim. Biophys. Acta 1056*, 259−272.
75. Schoepp, B., Parot, P., Lavorel, J., and Vermeglio, A. (1992) Charges recombination kinetics in bacterial photosynthetic reaction centers: Conformational states in equilibrium preexist in the dark, In *The Photosynthetic Bacterial Reaction Center II: Structure, Spectroscopy, and Dynamics* (Breton, J., and Vermeglio, A., Eds.) pp 331−339, Plenum Press, New York.
76. Baciou, L., and Sebban, P. (1995) Heterogeneity of the quinone electron acceptor system in bacterial reaction centers, *Photochem. Photobiol. 62*, 271−278.
77. Tiede, D. M., and Hanson, D. K. (1992) Protein relaxation following quinone reduction in *Rhodobacter capsulatus*: Detection of likely protonation-linked optical absorbance changes of the chromatophores, In *The Photosynthetic Bacterial Reaction Center II* (Breton, J., and Vermeglio, A., Eds.) pp 341−350, Plenum, New York.
78. Tiede, D. M., Utschig, L., Hanson, D. K., and Gallo, D. M. (1998) Resolution of electron and proton-transfer events in the electrochromism associated with quinone reduction in bacterial reaction centers, *Photosyn. Res. 55*, 267−273.
79. Kálmán, L., and Maróti, P. (1997) Conformation-activated protonation in reaction centers of the photosynthetic bacterium *Rhodobacter sphaeroides*, *Biochemistry 36*, 15269−15276.
80. Turzo, K., Laczko, G., and Maróti, P. (1999) Proton binding is part of protein relaxation of flash-excited reaction center from photosynthetic bacteria *Rhodobacter sphaeroides*, *Isr. J. Chem. 39*, 447−455.
81. Miksovska, J., Schiffer, M., Hanson, D. K., and Sebban, P. (1999) Proton uptake by bacterial reaction centers: The protein complex responds in a manner similar to the reduction of either quinone acceptor, *Proc. Natl. Acad. Sci. U.S.A. 96*, 14348−14353.
82. Utschig, L. M., Poluektov, O., Schlesselman, S. L., Thurnauer, M. C., and Tiede, D. M. (2001) Cu^{2+} site in photosynthetic bacterial reaction centers from *Rhodobacter sphaeroides*, *Rhodobacter capsulatus*, and *Rhodopseudomonas viridis*, *Biochemistry 40*, 6132−6141.
83. Xu, Q., and Gunner, M. R. (2002) Exploring the energy profile of the Q_A^- to Q_B electron-transfer reaction in bacterial photosynthetic reaction centers: pH dependence of the conformational gating step, *Biochemistry 41*, 2694−2701.
84. Xu, Q., Baciou, L., Sebban, P., and Gunner, M. R. (2002) Exploring the energy landscape for Q_A^- to Q_B electron transfer in bacterial photosynthetic reaction centers: effect of substrate position and tail length on the conformational gating step, *Biochemistry 41*, 10021−10025.
85. Stowell, M. H. B., McPhillips, T. M., Rees, D. C., Soltis, S. M., Abresch, E., and Feher, G. (1997) Light-induced structural changes in photosynthetic reaction center: Implications for mechanism of electron−proton transfer, *Science 276*, 812−816.
86. McAuley, K. E., Fyfe, P. K., Ridge, J. R., Isaacs, N. W., Cogdell, R. J., and Jones, M. R. (1999) Structural details of an interaction between cardiolipin and an integral membrane protein, *Proc. Natl. Acad. Sci. U.S.A. 96*, 14706−14711.
87. Pokkuluri, P. R., Laible, P. D., Deng, Y. L., Wong, T. N., Hanson, D. K., and Schiffer, M. (2002) The structure of a mutant photosynthetic reaction center shows unexpected changes in main chain orientations and quinone position, *Biochemistry 41*, 5998−6007.
88. Fritzsch, G., Koepke, J., Diem, R., Kuglstatter, A., and Baciou, L. (2002) Charge separation induces conformational changes in the photosynthetic reaction centre of purple bacteria, *Acta Crystallogr. D 58*, 1660−1663.
89. Kleinfeld, D., Okamura, M. Y., and Feher, G. (1984) Electron-transfer kinetics in photosynthetic reaction centers cooled to cryogenic temperatures in the charge-separated state: Evidence for light-induced structural changes, *Biochemistry 23*, 5780−5786.
90. Graige, M. S., Feher, G., and Okamura, M. Y. (1998) Conformational gating of the electron-transfer reaction $Q_A^-Q_B^- \rightarrow Q_AQ_B^-$ in bacterial reaction centers of *Rhodobacter sphaeroides* determined by a driving force assay, *Proc. Natl. Acad. Sci. U.S.A. 95*, 11679−11684.
91. Li, J., Takahashi, E., and Gunner, M. R. (2000) ΔG^o_{AB} and pH dependence of the electron transfer from $P^+Q_A^-Q_B$ to $P^+Q_AQ_B^-$ in *Rhodobacter sphaeroides* reaction centers, *Biochemistry 39*, 7445−7454.
92. Kuglstatter, A., Ermler, U., Michel, H., Baciou, L., and Fritzsch, G. (2001) X-ray structure analyses of photosynthetic reaction center variants from *Rhodobacter sphaeroides*: Structural changes induced by point mutations at position L209 modulate electron and proton transfer, *Biochemistry 40*, 4253−4260.

BI026959B